

Measurement of the cross-section for the process $\gamma^*\gamma^* \rightarrow$ hadrons at LEP

M. Acciarri, P. Achard, O. Adriani, M. Aguilar-Benitez, J. Alcaraz, G.
Alemanni, J. Allaby, A. Aloisio, M G. Alviggi, G. Ambrosi, et al.

► **To cite this version:**

M. Acciarri, P. Achard, O. Adriani, M. Aguilar-Benitez, J. Alcaraz, et al.. Measurement of the cross-section for the process $\gamma^*\gamma^* \rightarrow$ hadrons at LEP. Physics Letters B, Elsevier, 1999, 453, pp.333-342. in2p3-00003489

HAL Id: in2p3-00003489

<http://hal.in2p3.fr/in2p3-00003489>

Submitted on 1 Jun 1999

HAL is a multi-disciplinary open access archive for the deposit and dissemination of scientific research documents, whether they are published or not. The documents may come from teaching and research institutions in France or abroad, or from public or private research centers.

L'archive ouverte pluridisciplinaire **HAL**, est destinée au dépôt et à la diffusion de documents scientifiques de niveau recherche, publiés ou non, émanant des établissements d'enseignement et de recherche français ou étrangers, des laboratoires publics ou privés.

Measurement of the cross-section for the process
 $\gamma^*\gamma^* \rightarrow \text{hadrons}$ at LEP

The L3 Collaboration

Abstract

Measurements of the two-photon interaction $e^+e^- \rightarrow e^+e^- + \text{hadrons}$ at $\sqrt{s} \simeq 91$ GeV and $\sqrt{s} \simeq 183$ GeV are presented. The double-tag events, collected with the L3 detector, correspond to integrated luminosities of 140 pb^{-1} at 91 GeV and 52 pb^{-1} at 183 GeV. The cross-section of $\gamma^*\gamma^*$ collisions has been measured at $\langle Q^2 \rangle = 3.5 \text{ GeV}^2$ and $\langle Q^2 \rangle = 14 \text{ GeV}^2$. The data agree well with predictions based on perturbative QCD, while the Quark Parton Model alone is insufficient to describe the data.

Submitted to *Phys. Lett. B*

1 Introduction

We present the analysis of double-tag two-photon events, $e^+e^- \rightarrow e^+e^- + \text{hadrons}$, obtained at LEP with the L3 detector. The data, collected at centre-of-mass energies $\sqrt{s} \simeq 91$ GeV and $\sqrt{s} \simeq 183$ GeV, correspond to integrated luminosities of 140 pb^{-1} and 52 pb^{-1} , respectively. Both scattered electrons¹⁾ are detected in the small angle electromagnetic calorimeters. The virtuality of the two photons, Q_1^2 and Q_2^2 , is in the range of $1.2 \text{ GeV}^2 < Q_{1,2}^2 < 9 \text{ GeV}^2$ at $\sqrt{s} \simeq 91$ GeV and $2.5 \text{ GeV}^2 < Q_{1,2}^2 < 35 \text{ GeV}^2$ at $\sqrt{s} \simeq 183$ GeV. The centre-of-mass energy of the two virtual photons, $\sqrt{\hat{s}} = W_{\gamma\gamma}$, ranges from 2 GeV to 70 GeV.

For $Q_1^2 \approx Q_2^2 \approx 0$ untagged events [1], the two-photon cross-section, $\sigma_{\gamma\gamma}$, is dominated by vector-vector interactions, VDM (Fig. 1a). With increasing Q^2 , the VDM process is suppressed by the vector meson form factor and the Quark Parton Model process (QPM), shown in Fig. 1b, (also including QCD corrections) becomes important. Single-tag two-photon events, where $Q_1^2 \gg Q_2^2 \approx 0$, are usually analysed within the deep inelastic scattering formalism [2] and a photon structure function is introduced, in analogy to the proton structure function. Since the photon, unlike the proton, does not contain constituent quarks with an unknown density distribution, one may hope to have a complete QCD calculation under particular kinematical conditions.

Recently the highly virtual two-photon process, with $Q_1^2 \simeq Q_2^2$, has been considered as the “golden” process where the calculation can be verified without phenomenological inputs [3, 4]. The $\gamma^*\gamma^*$ interaction can be seen as the interaction of two $q\bar{q}$ pairs scattering off each other via multiple gluon exchange (Fig. 1c). For $\ln \hat{s}/Q^2 \approx 1$ a diagram with one-gluon exchange could be sufficient and the cross-section would be constant (Fig. 1d). In the limit of high energy, $\ln \hat{s}/Q^2 \gg 1$, the diagram of Fig. 1c is calculable by the resummation of the large logarithms, expressed by the BFKL equation [5]. In this scheme the cross-section for the collision of two virtual photons is [3, 4]:

$$\sigma_{\gamma^*\gamma^*} = \frac{\sigma_0}{Q_1 Q_2 \sqrt{Y}} \left(\frac{s}{s_0} \right)^{\alpha_P - 1} \approx \frac{\sigma_0}{Q_1 Q_2 \sqrt{Y}} \left(\frac{\hat{s}}{Q_1 Q_2} \right)^{\alpha_P - 1}. \quad (1)$$

Here

$$\begin{aligned} \sigma_0 &= \text{const} \\ s_0 &= \frac{Q_1 Q_2}{y_1 y_2}, \quad Y = \ln(s/s_0) \\ y_i &= 1 - (E_i/E_b) \cos^2(\theta_i/2) \end{aligned} \quad (2)$$

where E_b is the beam energy, E_i and θ_i are the energy and polar angle of the scattered electrons and α_P is the “hard Pomeron” intercept. The centre-of-mass energy of the two-photon system is related to the e^+e^- centre-of-mass energy s by $\hat{s} = W_{\gamma\gamma}^2 \approx s y_1 y_2$. In leading order one has $\alpha_P - 1 = (4 \ln 2) N_c \alpha_s / \pi$ where N_c is the number of colours. Using $N_c = 3$ and $\alpha_s = 0.2$, one obtains $\alpha_P - 1 \simeq 0.53$ [3, 4].

The double-tag interactions have been measured in previous experiments [6] at lower values of Q^2 and $W_{\gamma\gamma}$. For comparison with the prediction of the BFKL models, the cross-sections will be given as a function of the variable Y instead of $W_{\gamma\gamma}$ as used in Ref. [1, 6].

¹⁾Electron stands for electron or positron throughout this paper.

2 Monte Carlo Generators

Two different Monte Carlo generators are used in this analysis: PHOJET [7] and TWOGAM [8]. Both give a good description of the single-tag events [2] and use the GRV-LO [9] parton density in the photon to initiate QCD processes.

PHOJET is an event generator for pp , γp and quasi-real two-photon interactions, described within the Dual Parton Model. A transverse momentum cutoff, $p_t^{cut} = 2.5$ GeV, is applied to the partons of the resolved photons to separate soft from hard processes [10]. The complete lepton-photon vertex for transversely polarised photons is simulated. PHOJET gives also a good description of the untagged $\gamma\gamma \rightarrow$ hadrons events [1].

TWOGAM generates three different processes separately: the Vector Dominance Model, the Quark Parton Model and the QCD resolved photon contribution. The VDM part is generated according to Ref. [11]:

$$\sigma_{\gamma\gamma}(W_{\gamma\gamma}, Q_1^2, Q_2^2) = \sum_{i=T,L} F_i(Q_1^2) \cdot F_i(Q_2^2) \cdot \sigma_{\gamma\gamma}(W_{\gamma\gamma}) \quad (3)$$

where T (transverse) and L (longitudinal) are the polarisation indices of the virtual photon. The generalised VDM form factor [12] F_i describes the Q^2 dependence. For $\sigma_{\gamma\gamma}(W_{\gamma\gamma})$, we use our total cross-section measurement [1]. The QCD contribution of TWOGAM has been tuned to describe our measurement of single-tag events [2].

The dominant backgrounds are $e^+e^- \rightarrow e^+e^-\tau^+\tau^-$, simulated by JAMVG [13], and single-tag two-photon hadronic events, where a hadron is misidentified as a scattered electron. The contamination by annihilation processes is simulated by PYTHIA [14] ($e^+e^- \rightarrow$ hadrons), KORALZ [15] ($e^+e^- \rightarrow \tau^+\tau^-$) and KORALW [16] ($e^+e^- \rightarrow W^+W^-$).

All Monte Carlo events are passed through a full detector simulation using the GEANT [17] and the GEISHA [18] programs and are reconstructed in the same way as the data.

3 Data Analysis

3.1 Event Selection

A detailed description of the L3 detector is given in Ref. [19, 20]. The two-photon hadronic events are mainly triggered by two independent triggers: the central track [21] and the energy [22] triggers. The total trigger efficiency of the selected events is $\simeq 100\%$ at both beam energies.

Two-photon hadronic event candidates, $e^+e^- \rightarrow e^+e^- +$ hadrons, are selected using the following cuts:

- There must be two identified electrons, forward and backward (double-tag), in the small angle electromagnetic calorimeters. Each electron is identified as the highest energy cluster in one of the calorimeters, with energy greater than 30 GeV for $\sqrt{s} \simeq 91$ GeV and 40 GeV for $\sqrt{s} \simeq 183$ GeV. The polar angle of the two tagged electrons has to be in the range $30 \text{ mrad} < \theta_1 < 66 \text{ mrad}$ and $30 \text{ mrad} < \pi - \theta_2 < 66 \text{ mrad}$.
- The number of tracks must be greater than two. The tracks are required to have a transverse momentum, p_t , greater than 100 MeV and a distance of closest approach in the transverse plane to the interaction vertex smaller than 10 mm.

- The visible invariant mass, W_{vis} , of the hadronic final state is required to be larger than 2 GeV. The calculation of W_{vis} includes tracks, assumed to be pions, and isolated neutral energy clusters in the electromagnetic calorimeters with energies greater than 100 MeV.
- The value of $Y = \ln(s/s_0)$ is required to be in the range $2 \leq Y \leq 6$.

After these cuts, 137 events are selected at $\sqrt{s} \simeq 91$ GeV and 34 events at $\sqrt{s} \simeq 183$ GeV. The estimated backgrounds are listed in Table 1. The dominant background is $e^+e^- \rightarrow e^+e^-\tau^+\tau^-$ at 91 GeV and misidentified single-tag events at 183 GeV. The background from single-tag events is higher at 183 GeV because the energy cut on tagged electrons is much lower relative to the beam energy. The contamination from annihilation processes is negligible at both energies.

The distributions of Q_i^2 , y_i and E_i of the two scattered electrons are shown in Fig. 2 and Fig. 3. In Fig. 4, the distributions of $W_{\gamma\gamma}$ and Y are presented. The variable $W_{\gamma\gamma}$ is calculated using the kinematics of the two scattered electrons, taking advantage of the good resolution of the energy of scattered electrons (about 1.3% [20]). The resolution on $W_{\gamma\gamma}$ is about 18% at $W_{\gamma\gamma}/\sqrt{s} = 0.08$ and about 6% at $W_{\gamma\gamma}/\sqrt{s} = 0.2$. Both PHOJET and TWOGAM give a reasonable description of the shape of data at both beam energies. TWOGAM agrees well with the data also in absolute normalisation. The absolute normalisation of PHOJET is correct at $\sqrt{s} \simeq 183$ GeV, but is about 40% too low at $\sqrt{s} \simeq 91$ GeV.

Contrary to the case of untagged or single-tag events the $W_{\gamma\gamma}$ measurement does not rely on the W_{vis} measurement. The analysis is, therefore, less dependent on the Monte Carlo modelling of the structure of the final state.

3.2 Double-tag cross-section

The cross-sections are measured in the kinematic region limited by:

- $E_{1,2} > 30$ GeV, $30 \text{ mrad} < \theta_1 < 66 \text{ mrad}$ and $30 \text{ mrad} < \pi - \theta_2 < 66 \text{ mrad}$.
- $2 \leq Y \leq 6$.

The data are corrected for efficiency and acceptance with TWOGAM. The correction factors vary from about 30% at low values of Y to about 80% at high values of Y . The correction factors calculated with PHOJET are similar. The differential cross-sections $d\sigma(e^+e^- \rightarrow e^+e^- + \text{hadrons})/dY$ are measured in three ΔY intervals. They are listed in Table 2.

The systematic error due to the selection cuts is 5% for both beam energies, estimated by varying the cuts. The uncertainties on the cross-section from the background estimation of single-tag events are 2% at 91 GeV and 11% at 183 GeV. The uncertainties due to the acceptance correction are 9%, estimated by comparing TWOGAM and PHOJET. The different systematic uncertainties are added in quadrature to give the total systematic error listed in Table 2.

As can be seen in Table 2 and in Fig. 5, the QPM cross-section, estimated with JAMVG, lies below the data. The predictions of QCD Monte Carlo models implemented in TWOGAM and PHOJET are also listed in Table 2 and shown in Fig. 5. TWOGAM gives the best overall description. PHOJET lies below the data at $\sqrt{s} \simeq 91$ GeV, in particular in the low Y region. In the measured kinematical region the VDM contribution is small and the QCD contribution dominates at large values of Y .

From the measurement of the $e^+e^- \rightarrow e^+e^- + \text{hadrons}$ cross-section, σ_{ee} , we extract the two-photon cross-section, $\sigma_{\gamma^*\gamma^*}$, by using only the transverse photon luminosity function [23,24],

$\sigma_{ee} = L_{TT} \cdot \sigma_{\gamma^*\gamma^*}$. This measurement gives an effective cross-section containing contributions from transverse (T) and longitudinal (L) photon polarisations:

$$\sigma_{\gamma^*\gamma^*} = \sigma_{TT} + \epsilon_1\sigma_{TL} + \epsilon_2\sigma_{LT} + \epsilon_1\epsilon_2\sigma_{LL} \quad \epsilon_i = \frac{L_L}{L_T} = \frac{2(1-y_i)}{1+(1-y_i)^2} \quad (4)$$

where ϵ_i is the ratio of transverse and longitudinal photon luminosity functions. In the present kinematical region the values of ϵ_i are greater than 0.97, but the values of σ_{TL} , σ_{LT} and σ_{LL} are expected to be small [3]. The values of the two-photon cross-sections are given in Table 3.

In Fig. 6 we show $\sigma_{\gamma^*\gamma^*}$, after subtraction of the QPM contribution given in Table 2, as a function of Y . Using an average value of Q^2 , $\langle Q^2 \rangle = 3.5 \text{ GeV}^2$ at $\sqrt{s} \simeq 91 \text{ GeV}$ and $\langle Q^2 \rangle = 14 \text{ GeV}^2$ at $\sqrt{s} \simeq 183 \text{ GeV}$, we calculate the one-gluon exchange contribution with the asymptotic formula (Eq. 10.2 of Ref. [3]). The expectations are below the data. The leading order expectations of the BFKL model (Eq. 4.19 of Ref. [3]), shown as a dotted line in Fig. 6, are too high. By leaving α_P as a free parameter, a fit to the data, taking into account the statistical and systematic errors, yields:

$$\begin{aligned} \alpha_P - 1 &= 0.28 \pm 0.05 \quad \text{at } \sqrt{s} \simeq 91 \text{ GeV} \quad ; \\ \alpha_P - 1 &= 0.40 \pm 0.07 \quad \text{at } \sqrt{s} \simeq 183 \text{ GeV} \quad . \end{aligned} \quad (5)$$

The results are shown in Fig. 6 as a continuous line.

4 Conclusions

The cross-sections of double-tag $e^+e^- \rightarrow e^+e^- + \text{hadrons}$ events are measured at $\sqrt{s} \simeq 91 \text{ GeV}$ and $\sqrt{s} \simeq 183 \text{ GeV}$. They are well described by the TWOGAM Monte Carlo model which uses the GRV-LO parton density in the photon and leading order perturbative QCD. At $\sqrt{s} \simeq 91 \text{ GeV}$, the fitted value of $\alpha_P - 1$ is not in agreement with that expected from the BFKL model ($\alpha_P - 1 \simeq 0.53$). The disagreement becomes less visible at $\sqrt{s} \simeq 183 \text{ GeV}$.

Acknowledgements

We wish to thank A. De Roeck and D.E. Soper for very useful discussions. We express our gratitude to the CERN accelerator divisions for the excellent performance of the LEP machine. We acknowledge with appreciation the effort of all engineers, technicians and support staff who have participated in the construction and maintenance of this experiment.

References

- [1] L3 Coll., M. Acciarri *et al.*, Phys. Lett. **B 408** (1997) 450.
- [2] L3 Coll., M. Acciarri *et al.*, Phys. Lett. **B 436** (1998) 403;
L3 Coll., M. Acciarri *et al.*, Preprint CERN-EP/98-168, Phys. Lett. B accepted.
- [3] S.J. Brodsky, F. Hautmann and D.E. Soper, Phys. Rev. **D 56** (1997) 6957.
- [4] J. Bartels, A. De Roeck and H. Lotter, Phys. Lett. **B 389** (1996) 742;
J. Bartels, A. De Roeck, C. Ewerz and H. Lotter, hep-ph/9710500.
- [5] E.A. Kuraev, L.N. Lipatov and V.S. Fadin, Sov. Phys. JETP **45** (1977) 199;
Ya.Ya. Balitski and L.N. Lipatov, Sov. J. Nucl. Phys. **28** (1978) 822.
- [6] TPC/2 γ Coll., D. Bintinger *et al.*, Phys. Rev. Lett. **54** (1985) 763;
MD-1 Coll., S.E. Baru *et al.*, Z. Phys. **C 53** (1992) 219;
TOPAZ Coll., R. Enomoto *et al.*, Phys. Lett. **B 368** (1996) 299.
- [7] PHOJET version 1.05c is used.
R. Engel, Z. Phys. **C 66** (1995) 203;
R. Engel and J. Ranft, Phys. Rev. **D 54** (1996) 4244.
- [8] TWOGAM version 1.71 is used.
L. Lönnblad *et al.*, “ $\gamma\gamma$ event generators”, in Physics at LEP2, ed. G. Altarelli, T. Sjöstrand and F. Zwirner, CERN 96-01 (1996), Volume 2, 224.
S. Nova *et al.*, DELPHI Note 90-35 (1990).
We thank our colleagues from DELPHI to make their program available to us.
- [9] M. Glück, E. Reya and A. Vogt, Phys. Rev. **D 45** (1992) 3986;
M. Glück, E. Reya and A. Vogt, Phys. Rev. **D 46** (1992) 1973.
- [10] J.H. Field, F. Kapusta and L. Poggioli, Phys. Lett. **B 181** (1986) 362;
J.H. Field, F. Kapusta and L. Poggioli, Z. Phys. **C 36** (1987) 121.
- [11] I.F. Ginzburg and V.G. Serbo, Phys. Lett. **B 109** (1982) 231.
- [12] J.J. Sakurai and D. Schildknecht, Phys. Lett. **B 40** (1972) 121.
- [13] J.A.M. Vermaseren, Nucl. Phys. **B 229** (1983) 347.
- [14] T. Sjöstrand, Comp. Phys. Comm. **82** (1994) 74.
- [15] S. Jadach, B.F.L. Ward and Z. Wąs, Comp. Phys. Comm. **79** (1994) 503.
- [16] M. Skrzypek, S. Jadach, W. Placzek and Z. Wąs, Comp. Phys. Comm. **94** (1996) 216;
M. Skrzypek, S. Jadach, M. Martinez, W. Placzek and Z. Wąs, Phys. Lett. **B 372** (1996) 289.
- [17] R. Brun *et al.*, GEANT 3.15 preprint CERN DD/EE/84-1 (Revised 1987).
- [18] H. Fesefeldt, RWTH Aachen report PITHA 85/2 (1985).

- [19] L3 Collab., B. Adeva *et al.*, Nucl. Inst. Meth. **A 289** (1990) 35; M. Acciarri *et al.*, Nucl. Inst. Meth. **A 351** (1994) 300; M. Chemarin *et al.*, Nucl. Inst. Meth. **A 349** (1994) 345; A. Adam *et al.*, Nucl. Inst. Meth. **A 383** (1996) 342.
- [20] I.C. Brock *et al.*, Nucl. Inst. Meth. **A 381** (1996) 236.
- [21] P. Béné *et al.*, Nucl. Inst. Meth. **A 306** (1991) 150.
- [22] R. Bizzarri *et al.*, Nucl. Inst. Meth. **A 283** (1989) 799.
- [23] V.M. Budnev *et al.*, Phys. Rep. **C 15** (1975) 181.
- [24] G.A. Schuler, Improving the equivalent-photon approximation in electron-positron collisions, hep-ph/9610406.

We wish to thank the author for providing us with the numerical integration program of the luminosity function.

The L3 Collaboration:

M. Acciarri,²⁶ P. Achard,¹⁸ O. Adriani,¹⁵ M. Aguilar-Benitez,²⁵ J. Alcaraz,²⁵ G. Alemanni,²¹ J. Allaby,¹⁶ A. Aloisio,²⁸ M.G. Alvigi,²⁸ G. Ambrosi,¹⁸ H. Anderhub,⁴⁷ V.P. Andreev,^{6,36} T. Angelescu,¹² F. Anselmo,⁹ A. Arefiev,²⁷ T. Azemoon,³ T. Aziz,¹⁰ P. Bagnaia,³⁵ L. Baksay,⁴² A. Balandras,⁴ R.C. Ball,³ S. Banerjee,¹⁰ Sw. Banerjee,¹⁰ K. Banicz,⁴⁴ A. Barczyk,^{47,45} R. Barillere,¹⁶ L. Barone,³⁵ P. Bartalini,²¹ M. Basile,⁹ R. Battiston,³² A. Bay,²¹ F. Becattini,¹⁵ U. Becker,¹⁴ F. Behner,⁴⁷ J. Berdugo,²⁵ P. Berges,¹⁴ B. Bertucci,³² B.L. Betev,⁴⁷ S. Bhattacharya,¹⁰ M. Biasini,³² A. Biland,⁴⁷ J.J. Blaising,⁴ S.C. Blyth,³³ G.J. Bobbink,² A. Böhm,¹ L. Boldizsar,¹³ B. Borgia,^{16,35} D. Bourilkov,⁴⁷ M. Bourquin,¹⁸ S. Braccini,¹⁸ J.G. Branson,³⁸ V. Brigljevic,⁴⁷ F. Brochu,⁴ A. Buffini,¹⁵ A. Buijs,⁴³ J.D. Burger,¹⁴ W.J. Burger,³² J. Busenitz,⁴² A. Button,³ X.D. Cai,¹⁴ M. Campanelli,⁴⁷ M. Capell,¹⁴ G. Cara Romeo,⁹ G. Carlino,²⁸ A.M. Cartacci,¹⁵ J. Casaus,²⁵ G. Castellini,¹⁵ F. Cavallari,³⁵ N. Cavallo,²⁸ C. Cecchi,¹⁸ M. Cerrada,²⁵ F. Cesaroni,²² M. Chamizo,²⁵ Y.H. Chang,⁴⁹ U.K. Chaturvedi,¹⁷ M. Chemarin,²⁴ A. Chen,⁴⁹ G. Chen,⁷ G.M. Chen,⁷ H.F. Chen,¹⁹ H.S. Chen,⁷ X. Chereau,⁴ G. Chiefari,²⁸ L. Cifarelli,³⁷ F. Cindolo,⁹ C. Civinini,¹⁵ I. Clare,¹⁴ R. Clare,¹⁴ G. Coignet,⁴ A.P. Colijn,² N. Colino,²⁵ S. Costantini,⁸ F. Cotorobai,¹² B. de la Cruz,²⁵ A. Csilling,¹³ T.S. Dai,¹⁴ J.A. van Dalen,³⁰ R. D'Alessandro,¹⁵ R. de Asmundis,²⁸ P. Deglon,¹⁸ A. Degré,⁴ K. Deiters,⁴⁵ D. della Volpe,²⁸ P. Denes,³⁴ F. DeNotaristefani,³⁵ A. De Salvo,⁴⁷ M. Diemoz,³⁵ D. van Dierendonck,² F. Di Lodovico,⁴⁷ C. Dionisi,^{16,35} M. Dittmar,⁴⁷ A. Dominguez,³⁸ A. Doria,²⁸ M.T. Dova,^{17,4} D. Duchesneau,⁴ D. Dufournand,⁴ P. Duinker,² I. Duran,³⁹ H. El Mamouni,²⁴ A. Engler,³³ F.J. Eppling,¹⁴ F.C. Erné,² P. Extermann,¹⁸ M. Fabre,⁴⁵ R. Faccini,³⁵ M.A. Falagan,²⁵ S. Falciano,³⁵ A. Favara,¹⁵ J. Fay,²⁴ O. Fedin,³⁶ M. Felcini,⁴⁷ T. Ferguson,³³ F. Ferroni,³⁵ H. Fesefeldt,¹ E. Fiandrini,³² J.H. Field,¹⁸ F. Filthaut,¹⁶ P.H. Fisher,¹⁴ I. Fisk,³⁸ G. Forconi,¹⁴ L. Fredj,¹⁸ K. Freudenreich,⁴⁷ C. Furetta,²⁶ Yu. Galaktionov,^{27,14} S.N. Ganguli,¹⁰ P. Garcia-Abia,⁵ M. Gataullin,³¹ S.S. Gau,¹¹ S. Gentile,³⁵ N. Gheordanescu,¹² S. Giagu,³⁵ S. Goldfarb,²¹ Z.F. Gong,¹⁹ M.W. Gruenewald,⁸ R. van Gulik,² V.K. Gupta,³⁴ A. Gurtu,¹⁰ L.J. Gutay,⁴⁴ D. Haas,⁵ A. Hasan,²⁹ D. Hatzifotiadou,⁹ T. Hebbeker,⁸ A. Herve,¹⁶ P. Hidas,¹³ J. Hirschfelder,³³ H. Hofer,⁴⁷ G. Holzner,⁴⁷ H. Hoorani,³³ S.R. Hou,⁴⁹ I. Iashvili,⁴⁶ B.N. Jin,⁷ L.W. Jones,³ P. de Jong,¹⁶ I. Josa-Mutuberría,²⁵ R.A. Khan,¹⁷ D. Kamrad,⁴⁷ J.S. Kapustinsky,²³ M. Kaur,^{17,4} M.N. Kienzle-Focacci,¹⁸ D. Kim,³⁵ D.H. Kim,⁴¹ J.K. Kim,⁴¹ S.C. Kim,⁴¹ W.W. Kinnison,²³ J. Kirkby,¹⁶ D. Kiss,¹³ W. Kittel,³⁰ A. Klimentov,^{14,27} A.C. König,³⁰ A. Kopp,⁴⁶ I. Korolko,²⁷ V. Koutsenko,^{14,27} R.W. Kraemer,³³ W. Krenz,¹ A. Kunin,^{14,27} P. Lacentre,^{46,4,4} P. Ladrón de Guevara,²⁵ I. Laktineh,²⁴ G. Landi,¹⁵ C. Lapointe,¹⁴ K. Lassila-Perini,⁴⁷ P. Laurikainen,²⁰ A. Lavorato,³⁷ M. Lebeau,¹⁶ A. Lebedev,¹⁴ P. Lebrun,²⁴ P. Lecomte,⁴⁷ P. Lecoq,¹⁶ P. Le Coultre,⁴⁷ H.J. Lee,⁸ J.M. Le Goff,¹⁶ R. Leiste,⁴⁶ E. Leonardi,³⁵ P. Levchenko,³⁶ C. Li,¹⁹ C.H. Lin,⁴⁹ W.T. Lin,⁴⁹ F.L. Linde,^{2,16} L. Lista,²⁸ Z.A. Liu,⁷ W. Lohmann,⁴⁶ E. Longo,³⁵ Y.S. Lu,⁷ K. Lübelmeyer,¹ C. Luci,^{16,35} D. Luckey,¹⁴ L. Luminari,³⁵ W. Lustermann,⁴⁷ W.G. Ma,¹⁹ M. Maity,¹⁰ G. Majumder,¹⁰ L. Malgeri,¹⁶ A. Malinin,²⁷ C. Mañá,²⁵ D. Mangeol,³⁰ P. Marchesini,⁴⁷ G. Marian,^{42,4} J.P. Martin,²⁴ F. Marzano,³⁵ G.G.G. Massaro,² K. Mazumdar,¹⁰ R.R. McNeil,⁶ S. Mele,¹⁶ L. Merola,²⁸ M. Meschini,¹⁵ W.J. Metzger,³⁰ M. von der Mey,¹ D. Migani,⁹ A. Mihul,¹² H. Milcent,¹⁶ G. Mirabelli,³⁵ J. Mnich,¹⁶ P. Molnar,⁸ B. Monteleoni,¹⁵ T. Moulik,¹⁰ G.S. Muanza,²⁴ F. Muheim,¹⁸ A.J.M. Muijs,² S. Nahn,¹⁴ M. Napolitano,²⁸ F. Nessi-Tedaldi,⁴⁷ H. Newman,³¹ T. Niessen,¹ A. Nippe,²¹ A. Nisati,³⁵ H. Nowak,⁴⁶ Y.D. Oh,⁴¹ G. Organtini,³⁵ R. Ostonen,²⁰ C. Palomares,²⁵ D. Pandoulas,¹ S. Paoletti,^{35,16} P. Paolucci,²⁸ H.K. Park,³³ I.H. Park,⁴¹ G. Pascale,³⁵ G. Passaleva,¹⁶ S. Patricelli,²⁸ T. Paul,¹¹ M. Pauluzzi,³² C. Paus,¹⁶ F. Pauss,⁴⁷ D. Peach,¹⁶ M. Pedace,³⁵ Y.J. Pei,¹ S. Pensotti,²⁶ D. Perret-Gallix,⁴ B. Petersen,³⁰ S. Petrak,⁸ D. Piccolo,²⁸ M. Pieri,¹⁵ P.A. Piroué,³⁴ E. Pistolesi,²⁶ V. Plyaskin,²⁷ M. Pohl,⁴⁷ V. Pojidaev,^{27,15} H. Postema,¹⁴ J. Pothier,¹⁶ N. Produit,¹⁸ D. Prokofiev,³⁶ J. Quartieri,³⁷ G. Rahal-Callot,⁴⁷ N. Raja,¹⁰ P.G. Rancoita,²⁶ G. Raven,³⁸ P. Razis,²⁹ D. Ren,⁴⁷ M. Rescigno,³⁵ S. Reucroft,¹¹ T. van Rhee,⁴³ S. Riemann,⁴⁶ K. Riles,³ A. Robohm,⁴⁷ J. Rodin,⁴² B.P. Roe,³ L. Romero,²⁵ S. Rosier-Lees,⁴ J.A. Rubio,¹⁶ D. Ruschmeier,⁸ H. Rykaczewski,⁴⁷ S. Sakar,³⁵ J. Salicio,¹⁶ E. Sanchez,²⁵ M.P. Sanders,³⁰ M.E. Sarakinos,²⁰ C. Schäfer,¹ V. Schegelsky,³⁶ S. Schmidt-Kaerst,¹ D. Schmitz,¹ N. Scholz,⁴⁷ H. Schopper,⁴⁸ D.J. Schotanus,³⁰ J. Schwenke,¹ G. Schwering,¹ C. Sciacca,²⁸ D. Sciarrino,¹⁸ L. Servoli,³² S. Shevchenko,³¹ N. Shivarov,⁴⁰ V. Shoutko,²⁷ J. Shukla,²³ E. Shumilov,²⁷ A. Shvorob,³¹ T. Siedenburger,¹ D. Son,⁴¹ B. Smith,³³ P. Spillantini,¹⁵ M. Steuer,¹⁴ D.P. Stickland,³⁴ A. Stone,⁶ H. Stone,³⁴ B. Stoyanov,⁴⁰ A. Straessner,¹ K. Sudhakar,¹⁰ G. Sultanov,¹⁷ L.Z. Sun,¹⁹ H. Suter,⁴⁷ J.D. Swain,¹⁷ Z. Szillasi,^{42,4} X.W. Tang,⁷ L. Tauscher,⁵ L. Taylor,¹¹ C. Timmermans,³⁰ Samuel C.C. Ting,¹⁴ S.M. Ting,¹⁴ S.C. Tonwar,¹⁰ J. Tóth,¹³ C. Tully,³⁴ K.L. Tung,⁷ Y. Uchida,¹⁴ J. Ulbricht,⁴⁷ E. Valente,³⁵ G. Vesztegombi,¹³ I. Vetlitsky,²⁷ G. Viertel,⁴⁷ S. Villa,¹¹ M. Vivargent,⁴ S. Vlachos,⁵ H. Vogel,³³ H. Vogt,⁴⁶ I. Vorobiev,^{16,27} A.A. Vorobyov,³⁶ A. Vorvolakos,²⁹ M. Wadhwa,⁵ W. Wallraff,¹ J.C. Wang,¹⁴ X.L. Wang,¹⁹ Z.M. Wang,¹⁹ A. Weber,¹ M. Weber,¹ P. Wienemann,¹ H. Wilkens,³⁰ S.X. Wu,¹⁴ S. Wynhoff,¹ L. Xia,¹ Z.Z. Xu,¹⁹ B.Z. Yang,¹⁹ C.G. Yang,⁷ H.J. Yang,⁷ M. Yang,⁷ J.B. Ye,¹⁹ S.C. Yeh,⁵⁰ J.M. You,³³ An. Zalite,³⁶ Yu. Zalite,³⁶ P. Zemp,⁴⁷ Z.P. Zhang,¹⁹ G.Y. Zhu,⁷ R.Y. Zhu,³¹ A. Zichichi,^{9,16,17} F. Ziegler,⁴⁶ G. Zilizi,^{42,4} M. Zöller,¹

- 1 I. Physikalisches Institut, RWTH, D-52056 Aachen, FRG[§]
 - III. Physikalisches Institut, RWTH, D-52056 Aachen, FRG[§]
 - 2 National Institute for High Energy Physics, NIKHEF, and University of Amsterdam, NL-1009 DB Amsterdam, The Netherlands
 - 3 University of Michigan, Ann Arbor, MI 48109, USA
 - 4 Laboratoire d'Annecy-le-Vieux de Physique des Particules, LAPP, IN2P3-CNRS, BP 110, F-74941 Annecy-le-Vieux CEDEX, France
 - 5 Institute of Physics, University of Basel, CH-4056 Basel, Switzerland
 - 6 Louisiana State University, Baton Rouge, LA 70803, USA
 - 7 Institute of High Energy Physics, IHEP, 100039 Beijing, China[△]
 - 8 Humboldt University, D-10099 Berlin, FRG[§]
 - 9 University of Bologna and INFN-Sezione di Bologna, I-40126 Bologna, Italy
 - 10 Tata Institute of Fundamental Research, Bombay 400 005, India
 - 11 Northeastern University, Boston, MA 02115, USA
 - 12 Institute of Atomic Physics and University of Bucharest, R-76900 Bucharest, Romania
 - 13 Central Research Institute for Physics of the Hungarian Academy of Sciences, H-1525 Budapest 114, Hungary[‡]
 - 14 Massachusetts Institute of Technology, Cambridge, MA 02139, USA
 - 15 INFN Sezione di Firenze and University of Florence, I-50125 Florence, Italy
 - 16 European Laboratory for Particle Physics, CERN, CH-1211 Geneva 23, Switzerland
 - 17 World Laboratory, FBLJA Project, CH-1211 Geneva 23, Switzerland
 - 18 University of Geneva, CH-1211 Geneva 4, Switzerland
 - 19 Chinese University of Science and Technology, USTC, Hefei, Anhui 230 029, China[△]
 - 20 SEFT, Research Institute for High Energy Physics, P.O. Box 9, SF-00014 Helsinki, Finland
 - 21 University of Lausanne, CH-1015 Lausanne, Switzerland
 - 22 INFN-Sezione di Lecce and Università Degli Studi di Lecce, I-73100 Lecce, Italy
 - 23 Los Alamos National Laboratory, Los Alamos, NM 87544, USA
 - 24 Institut de Physique Nucléaire de Lyon, IN2P3-CNRS, Université Claude Bernard, F-69622 Villeurbanne, France
 - 25 Centro de Investigaciones Energéticas, Medioambientales y Tecnológicas, CIEMAT, E-28040 Madrid, Spain^b
 - 26 INFN-Sezione di Milano, I-20133 Milan, Italy
 - 27 Institute of Theoretical and Experimental Physics, ITEP, Moscow, Russia
 - 28 INFN-Sezione di Napoli and University of Naples, I-80125 Naples, Italy
 - 29 Department of Natural Sciences, University of Cyprus, Nicosia, Cyprus
 - 30 University of Nijmegen and NIKHEF, NL-6525 ED Nijmegen, The Netherlands
 - 31 California Institute of Technology, Pasadena, CA 91125, USA
 - 32 INFN-Sezione di Perugia and Università Degli Studi di Perugia, I-06100 Perugia, Italy
 - 33 Carnegie Mellon University, Pittsburgh, PA 15213, USA
 - 34 Princeton University, Princeton, NJ 08544, USA
 - 35 INFN-Sezione di Roma and University of Rome, "La Sapienza", I-00185 Rome, Italy
 - 36 Nuclear Physics Institute, St. Petersburg, Russia
 - 37 University and INFN, Salerno, I-84100 Salerno, Italy
 - 38 University of California, San Diego, CA 92093, USA
 - 39 Dept. de Física de Partículas Elementales, Univ. de Santiago, E-15706 Santiago de Compostela, Spain
 - 40 Bulgarian Academy of Sciences, Central Lab. of Mechatronics and Instrumentation, BU-1113 Sofia, Bulgaria
 - 41 Center for High Energy Physics, Adv. Inst. of Sciences and Technology, 305-701 Taejeon, Republic of Korea
 - 42 University of Alabama, Tuscaloosa, AL 35486, USA
 - 43 Utrecht University and NIKHEF, NL-3584 CB Utrecht, The Netherlands
 - 44 Purdue University, West Lafayette, IN 47907, USA
 - 45 Paul Scherrer Institut, PSI, CH-5232 Villigen, Switzerland
 - 46 DESY-Institut für Hochenergiephysik, D-15738 Zeuthen, FRG
 - 47 Eidgenössische Technische Hochschule, ETH Zürich, CH-8093 Zürich, Switzerland
 - 48 University of Hamburg, D-22761 Hamburg, FRG
 - 49 National Central University, Chung-Li, Taiwan, China
 - 50 Department of Physics, National Tsing Hua University, Taiwan, China
- [§] Supported by the German Bundesministerium für Bildung, Wissenschaft, Forschung und Technologie
[‡] Supported by the Hungarian OTKA fund under contract numbers T019181, F023259 and T024011.
[¶] Also supported by the Hungarian OTKA fund under contract numbers T22238 and T026178.
^b Supported also by the Comisión Interministerial de Ciencia y Tecnología.
[‡] Also supported by CONICET and Universidad Nacional de La Plata, CC 67, 1900 La Plata, Argentina.
[‡] Supported by Deutscher Akademischer Austauschdienst.
[◇] Also supported by Panjab University, Chandigarh-160014, India.
[△] Supported by the National Natural Science Foundation of China.

	91 GeV	183 GeV
Selected events	137	34
Single-tag	5.7 ± 1.8	3.2 ± 3.2
$e^+e^- \rightarrow e^+e^-\tau^+\tau^-$	7.1 ± 1.7	1.0 ± 0.4

Table 1: The numbers of selected signal and estimated background events.

91 GeV				
	Data	QPM	TWOGAM	PHOJET
ΔY	$d\sigma/dY$	$d\sigma/dY$	$d\sigma/dY$	$d\sigma/dY$
2 – 3	$1.02 \pm 0.14 \pm 0.11$	0.537	0.85	0.33
3 – 4	$0.43 \pm 0.06 \pm 0.05$	0.191	0.41	0.29
4 – 6	$0.14 \pm 0.03 \pm 0.01$	0.026	0.15	0.09
183 GeV				
	Data	QPM	TWOGAM	PHOJET
ΔY	$d\sigma/dY$	$d\sigma/dY$	$d\sigma/dY$	$d\sigma/dY$
2 – 3	$0.36 \pm 0.12 \pm 0.05$	0.181	0.31	0.32
3 – 4	$0.23 \pm 0.07 \pm 0.03$	0.066	0.21	0.25
4 – 6	$0.13 \pm 0.04 \pm 0.02$	0.012	0.19	0.17

Table 2: The differential cross-section, $d\sigma(e^+e^- \rightarrow e^+e^- + \text{hadrons})/dY$ in picobarn measured in the kinematic region defined in the text, at $\sqrt{s} \simeq 91$ GeV and $\sqrt{s} \simeq 183$ GeV. The first error is statistical and the second is systematic. The predictions of the QPM and the different Monte Carlo models are also listed.

	91 GeV	183 GeV
ΔY	$\sigma_{\gamma^*\gamma^*}$	$\sigma_{\gamma^*\gamma^*}$
2 – 3	$27 \pm 4 \pm 3$	$7.2 \pm 2.3 \pm 1.1$
3 – 4	$20 \pm 3 \pm 2$	$7.2 \pm 2.2 \pm 1.1$
4 – 6	$21 \pm 4 \pm 2$	$8.2 \pm 2.8 \pm 1.2$

Table 3: The two-photon cross-section, $\sigma_{\gamma^*\gamma^*}$ in nanobarn, as a function of Y at $\sqrt{s} \simeq 91$ GeV and $\sqrt{s} \simeq 183$ GeV. The first error is statistical and the second is systematic.

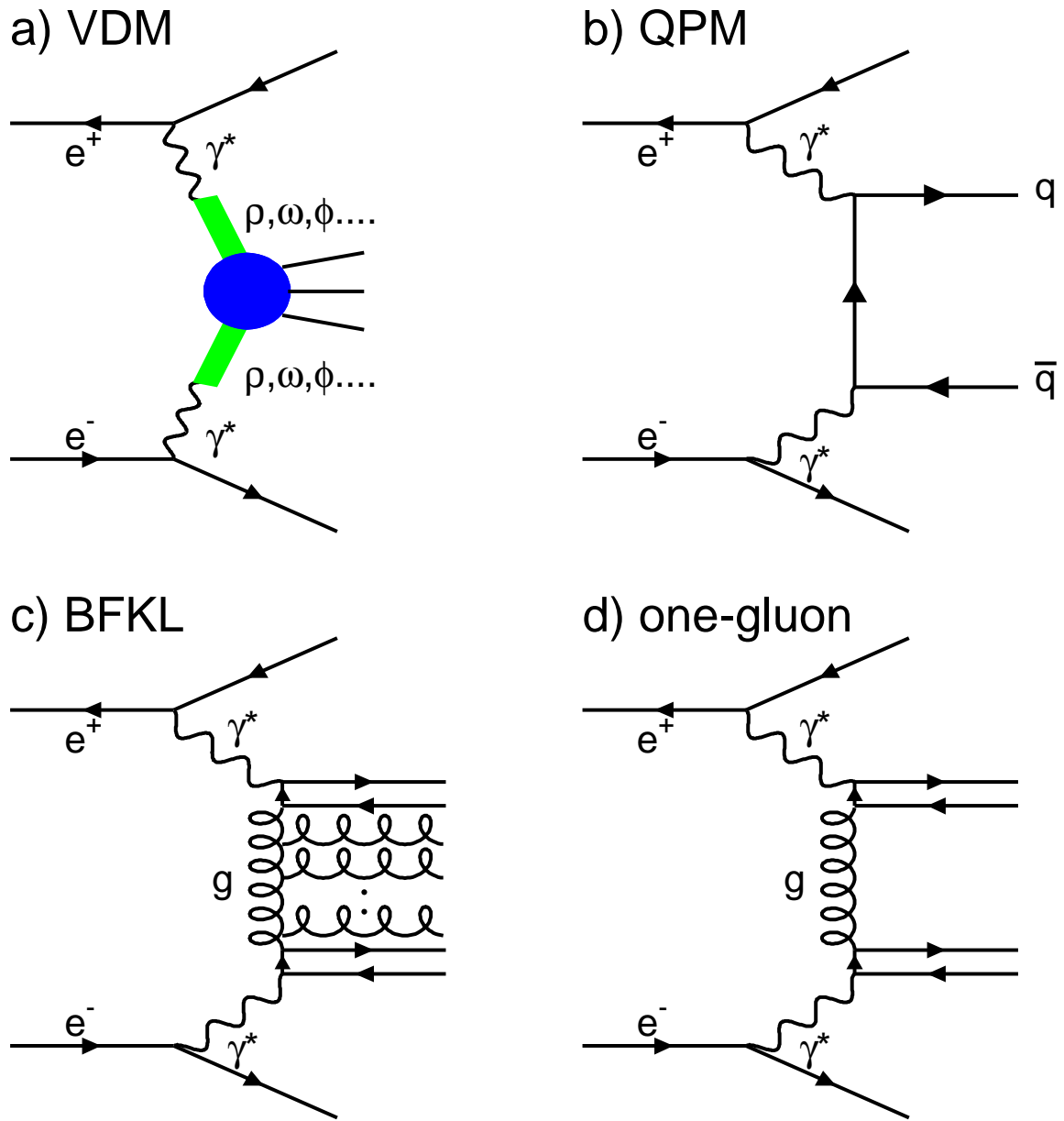


Figure 1: Diagrams for the a) VDM, b) QPM, c) BFKL Pomeron and d) one-gluon exchange processes in a $\gamma^*\gamma^*$ interaction.

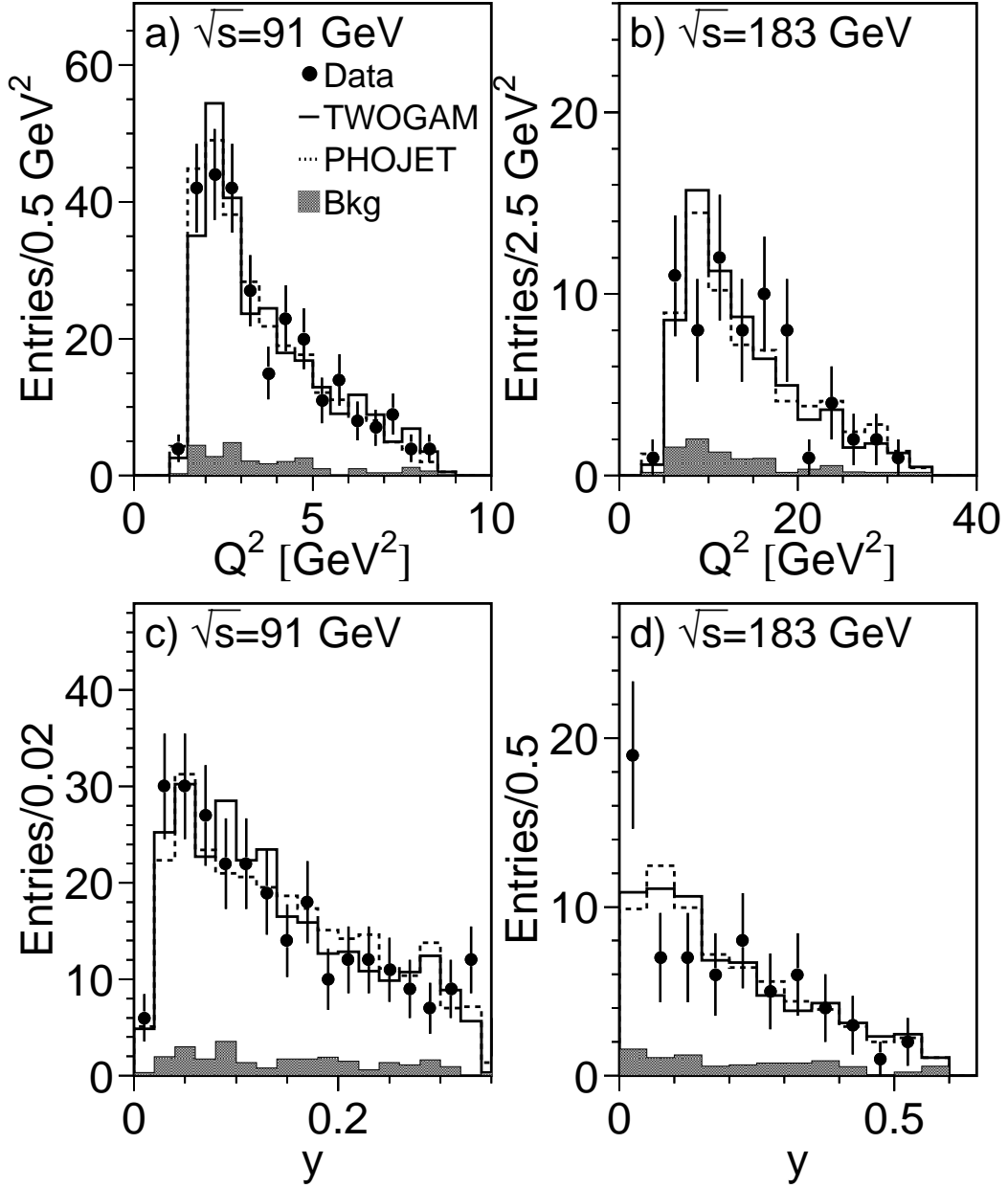


Figure 2: Distributions of Q^2 (a and b) and y (c and d) of scattered electrons. The data are compared to the Monte Carlo predictions, normalised to the number of data events after background subtraction. There are two entries per event.

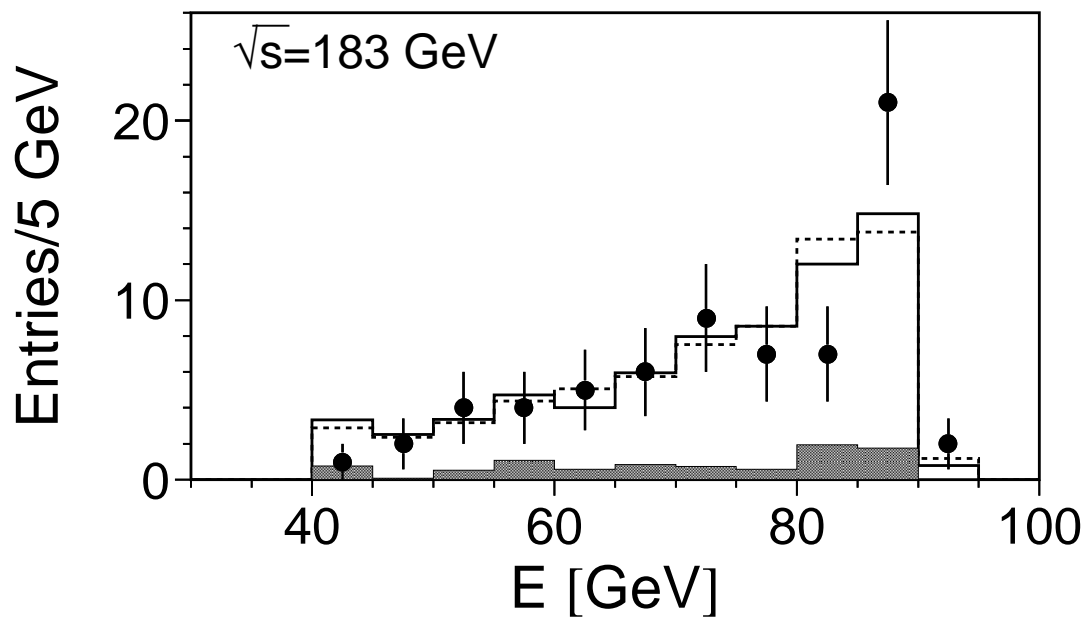
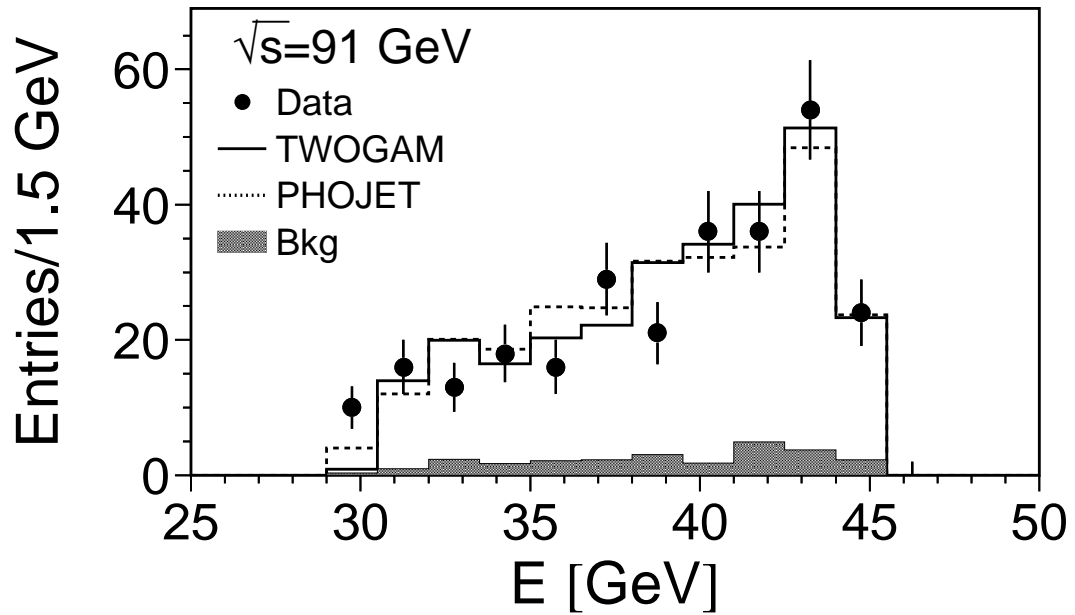


Figure 3: Distributions of the energies of the scattered electrons. The data are compared to the Monte Carlo predictions, normalised to the number of data events after background subtraction. There are two entries per event.

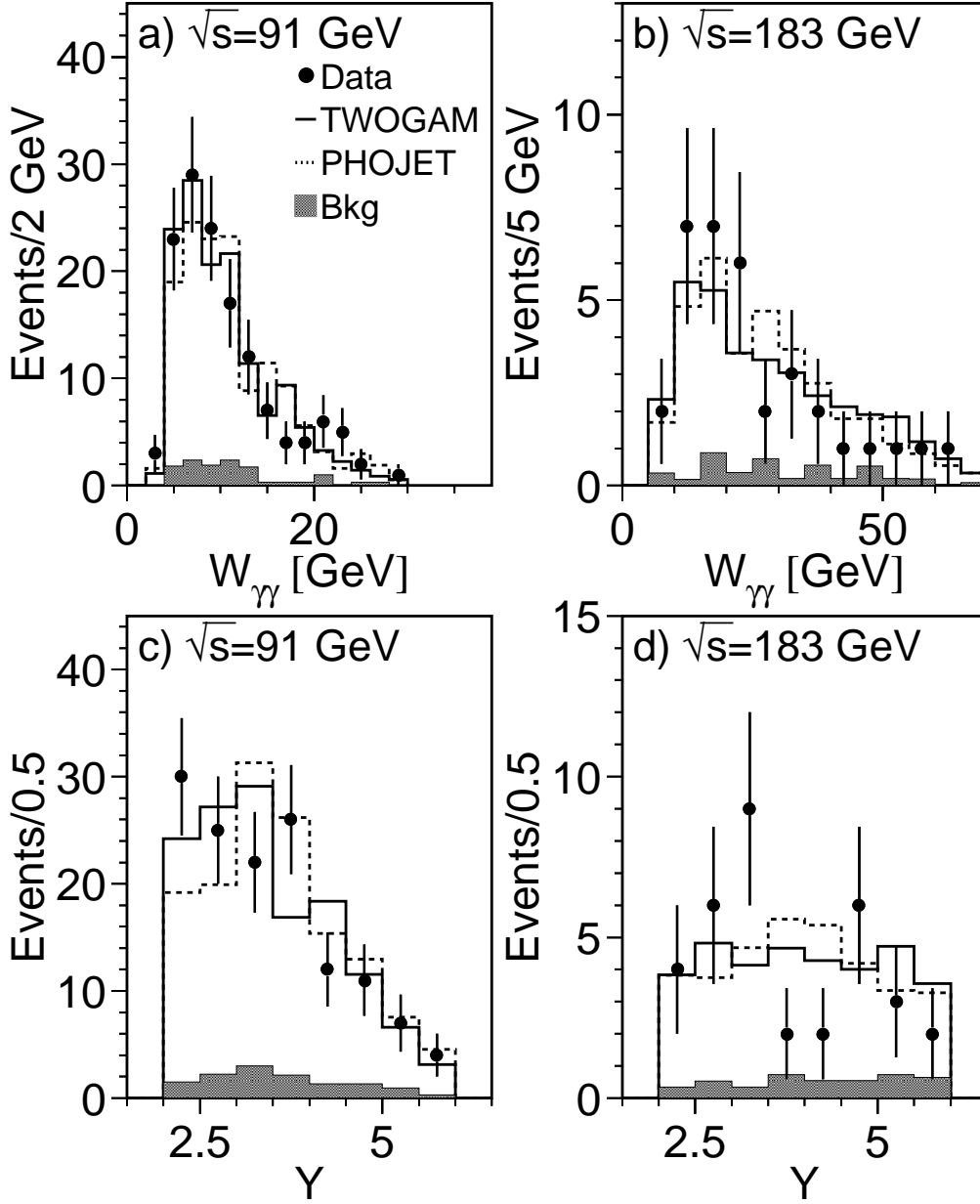


Figure 4: Distributions of the two-photon mass, $W_{\gamma\gamma}$, (a and b) and of the variable Y (c and d). The data are compared to the Monte Carlo predictions, normalised to the number of data events after background subtraction.

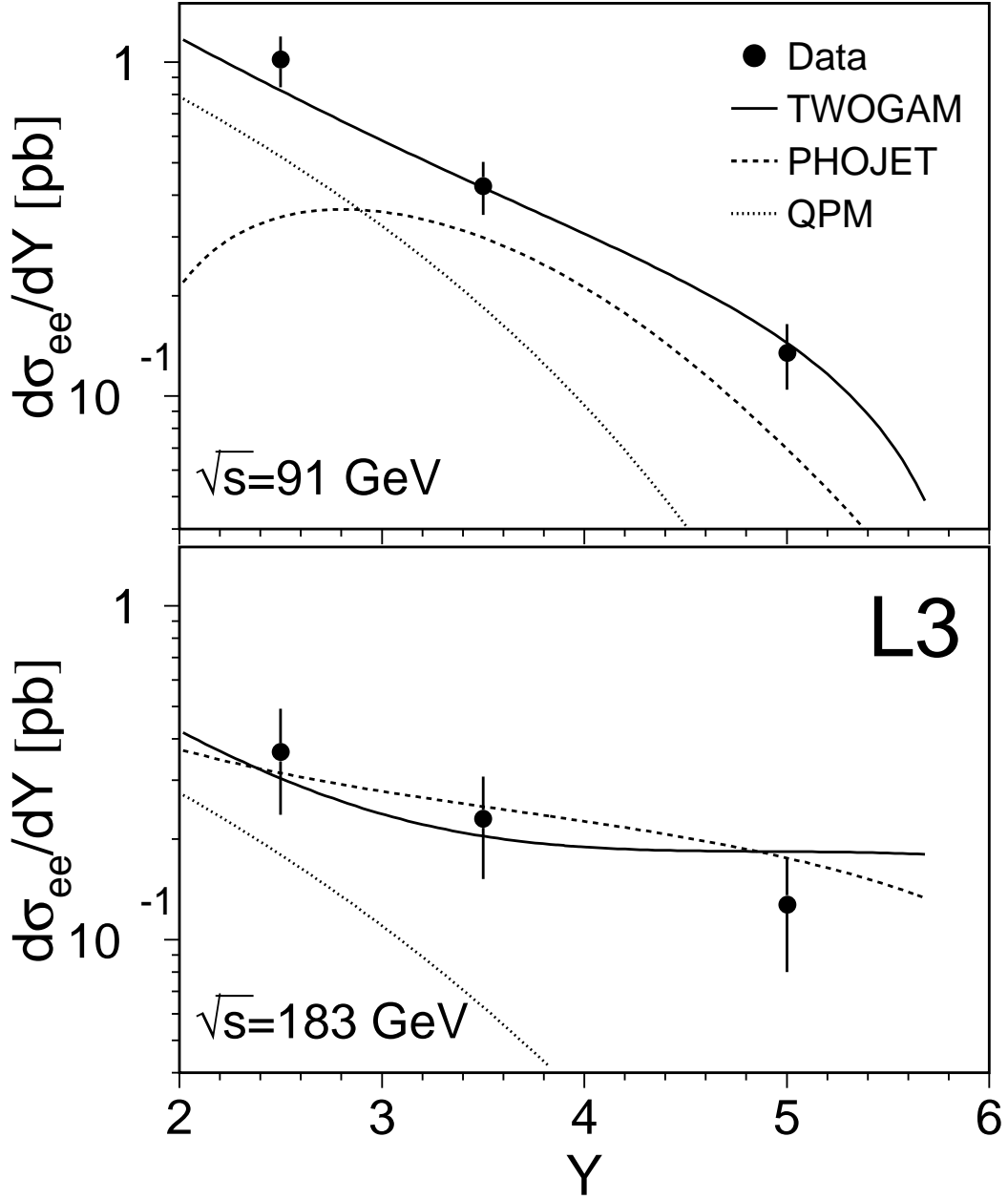


Figure 5: The cross-section of $e^+e^- \rightarrow e^+e^- + \text{hadrons}$ as a function of Y in the kinematical region defined in the text at $\sqrt{s} \simeq 91$ GeV and $\sqrt{s} \simeq 183$ GeV compared to the predictions of the Monte Carlo models and of QPM.

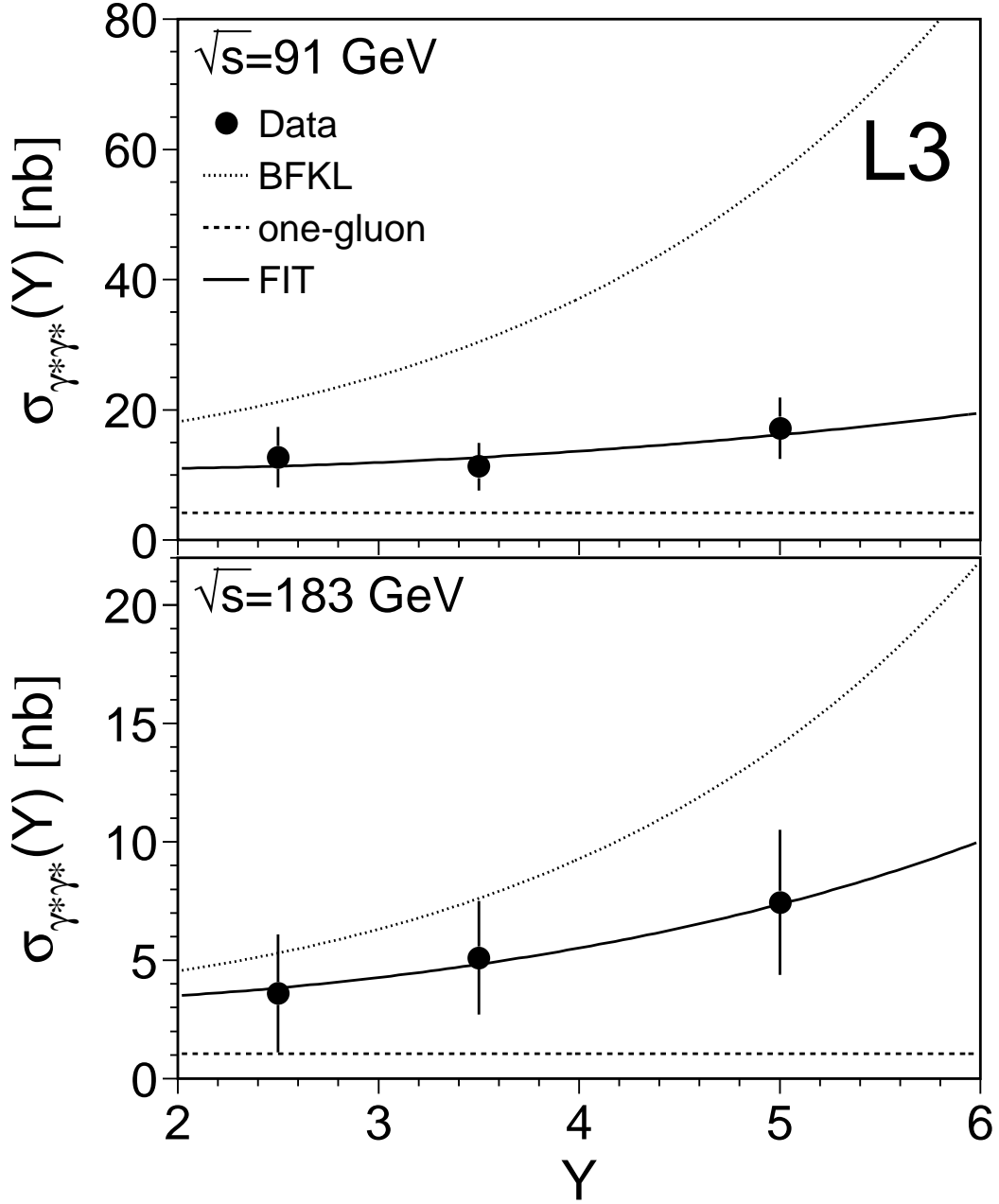


Figure 6: Two-photon cross-sections, $\sigma_{\gamma^*\gamma^*}$, after subtraction of the QPM contribution at $\sqrt{s} \simeq 91$ GeV ($\langle Q^2 \rangle = 3.5$ GeV²) and $\sqrt{s} \simeq 183$ GeV ($\langle Q^2 \rangle = 14$ GeV²). The data are compared to the predictions of the BFKL model and of the one-gluon exchange diagram. The continuous line is a fit to the data with Eq. 1 by leaving α_P as a free parameter.